Arabian Journal of Geosciences (2018) 11: 325
https://doi.org/10.1007/s12517-018-3685-1

ORIGINAL PAPER

Development and verification of the comprehensive model for physical properties of hydrate sediment

Qingchao Li[1] · Yuanfang Cheng[1] · Qiang Li[1] · Ubedullah Ansari[1] · Yuwen Liu[1] · Chuanliang Yan[1] · Chuang Lei[1,2]

Received: 11 December 2017 / Accepted: 14 June 2018 / Published online: 25 June 2018

Abstract

Natural gas hydrate is widely distributed all over the world and may be a potential resource in the near future, whereas hydrate dissociation during the development affects wellbore stability and drilling safety. However, the present modeling of hydrate reservoir parameters ignored the influence of effective stress and only considered the hydrate saturation. In this paper, a series of stress sensitivity experiments for the unconsolidated sandstone were carried out, and the influence of mean effective stress on physical parameters was obtained; a comprehensive model for the physical parameters of hydrate reservoir was developed subsequently. With the help of ABAQUS finite element software, the established comprehensive model was verified by the use of the wellbore stability numerical model of hydrate reservoir. The verification results show that ignoring the effect of mean effective stress on the parameters of hydrate formation aggravates the invasion of drilling fluid into the hydrate formation. Besides, ignoring the stress sensitivity of reservoir physical parameters will underestimate the wellbore instability during hydrate drilling, which will be a threat to the safety of gas hydrate drilling. At the end of the drilling operation, the maximum plastic strain of the model for considering and not considering stress sensitivity was 0.0145 and 0.0138, respectively. Therefore, the established comprehensive model will provide a theoretical support for accurately predicting the engineering geological disasters in hydrate development process.

Keywords Stress sensitivity · Wellbore stability · Hydrate dissociation · Finite element simulation · Coupling of multi-physics fields

Introduction

Natural gas stored in hydrate sediments may be a potential resource in the near future because of the characteristics of both the massive reserve and the clean energy (Yan et al. 2017). Consequently, it is undeniable that the development and utilization of methane hydrate are attractive and drawing public attention (Sakamoto et al. 2007; Su et al. 2013; Moridis and Reagan 2007; Schnurle et al. 2002; Gai and Sánchez, 2017). At present, three main development methods are considered to be practical for producing natural gas from hydrate sediments: depressurization, thermal stimulation, and use of the inhibitor (Su et al. 2010; Su et al. 2013; Moridis and Reagan 2007; Bybee 2007). However, hydrate dissociation caused by different development methods may result in a series of engineering geological hazards (e.g., wellbore instability, formation subsidence, and submarine landslides) (Briaud and Chaouch 1997; Li et al. 2013; Liu et al. 2014; Qiu et al. 2015; Li et al. 2018), which will pose a danger to the environment and to the safety of human's lives. Experimental investigation of geological hazards that occurred during hydrate development is time consuming and costly, whereas numerical simulation is an effective and economical method to evaluate the probability of disaster occurrence. Furthermore, it is the basis of numerical simulation to obtain a comprehensive model that can reflect the variation law of physical parameters in hydrate dissociation.

Over the past few decades, numerous studies have been carried out to investigate the relationship between physical parameters of hydrate reservoirs and hydrate saturation, by

✉ Qingchao Li
1084346639@qq.com

Yuanfang Cheng
B16020225@s.upc.edu.cn

[1] School of Petroleum Engineering, China University of Petroleum (East China), Qingdao 266580, China

[2] PetroChina Huabei Oilfield Company, Renqiu 062500, China

using both experiments and logging data analysis (Minagawa et al. 2005; Klar and Soga 2005; Rutqvist and Moridis 2007; Yohan et al. 2016). Masuda et al. (1997) established a model for determining the relationship between the relative permeability of hydrate reservoir rocks and hydrate saturation, which is widely accepted by domestic and foreign scholars. In their model, the relative permeability of the hydrate reservoir decreases exponentially with the hydrate saturation. Minagawa et al. (2005) carried out a series of experiments and obtained the fitting formula between the intrinsic permeability of hydrate reservoirs and hydrate saturation; it showed that the intrinsic permeability exhibited an exponential relationship with the change of hydrate saturation. Klar et al. (2010) developed the best fit prediction model of mechanical parameters for hydrate sediment by simulation experiments of hydrate dissociation; the results showed that the internal friction angle and the Poisson's ratio are constant values, but the elastic modulus and cohesion are the linear functions of the hydrate saturation. Rutqvist and Moridis (2007) gave the relationship between the mechanical parameters and the hydrate saturation by fitting the experimental data performed by Masui et al. (2007) and summarizing the data from various literatures, and the similar results were presented with that of Klar et al. (2010). Besides, the similar conclusions have also been drawn by Ng et al. (2008) and Uchida et al. (2012). Besides, all these previous studies have been summarized and presented by Yohan et al. (2016) in their paper. In a word, these studies above are all valuable and have been used for investigating stratum deformation and stress distribution within the hydrate reservoirs during hydrate development from different perspectives. Both the dissociation effect of hydrate and the stress sensitivity of reservoirs are two important factors influencing the physical properties of hydrate reservoir (Cheng et al. 2010). However, nearly all the fore-mentioned studies have only considered the hydrate dissociation effect during hydrate development, and neglected the influence of stress variation during development on physical parameters. The deficiency of physical parameters model for hydrate sediment seriously restricts the accuracy and reliability of numerical simulation.

As mentioned above, the study of stress sensitivity plays an important role in analyses of reservoir deformation and wellbore stability, and some scholars have conducted investigations into the stress dependence of mechanical properties of hydrate sediment to a certain extent. Kwon et al. (2011) performed standard consolidation tests of undisturbed hydrate sediment cores and studied the effect of stresses on volume responses. The experimental analyses provide important geotechnical engineering parameters for numerical simulation. Kim et al. (2012) and Lee et al. (2013) carried out the experimental analyses of hydrate sediments recovered in expedition and gave the basic geotechnical properties. The experimental results showed that the shear wave velocities indicate high stress sensitivity, which indirectly indicates that the strength parameters of hydrate sediment are stress-dependent. Accordingly, it is of great significance to establish a comprehensive model that takes into account of both the hydrate dissociation effect and the stress sensitivity. However, these studies do not give quantitative relationships between the mechanical parameters of hydrate-bearing sediments and the effective stress.

By introducing both hydrate dissociation effect and stress sensitivity of hydrate reservoirs, a comprehensive model for physical parameters of the hydrate reservoirs was established on the basis of the triaxial experimental results. Meanwhile, a finite element model for studying the wellbore stability of hydrate sediment was established by coupling thermo-hydro-mechanical fields. Based on the numerical simulation results of the wellbore stability in hydrate formations, the applicability of the above-established comprehensive model is verified in detail. Thereby, the research in this paper can provide more accurate parameter model for the evaluation of engineering geological disasters and complex underground accidents in the process of hydrate development.

Experiment section

Experimental system

In order to satisfy the requirements of determining the physical parameters of the unconsolidated sandstone, an experimental system (Fig. 1) for studying the stress sensitivity of reservoirs was established. The system mainly consists of axial pressure loading system, confining pressure loading system, pore pressure loading system, and the servo-controlled system, as well as other devices for preparing the rock samples. The preparation of rock sample and the measurement of physical parameters are integrated into one single experimental system. With the help of the established experimental system, all physical parameters needed in numerical simulation can be measured simultaneously under loading conditions. The maximum confining pressure and maximum pore pressure that the experimental system can withstand are 100 and 60 MPa, respectively, which can fully meet the experimental requirements. The axial piston can achieve any displacement load within 100 mm with accuracy of ± 1%, and a load of up to 1000 KN can be applied to the rock sample in the axial direction. Two displacement gauges were used to measure the axial and radial displacements, and the maximum displacement that the displacement gauge can measure was 8 mm with the accuracy of up to ± 1 μm. Furthermore, three servo valves (servo valve − 1, servo valve − 2, servo valve − 3 in Fig. 1), which were controlled by the servo-controlled system, were

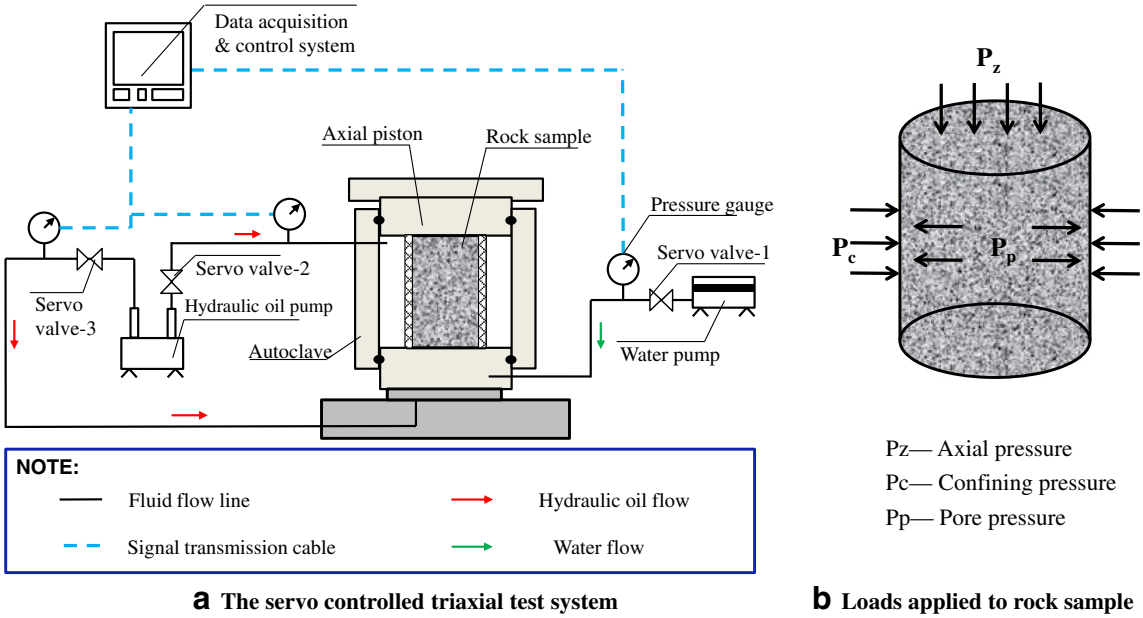

a The servo controlled triaxial test system **b** Loads applied to rock sample

Fig. 1 Sketch map of the servo-controlled triaxial experimental system for measuring properties of sample

used to control the pore pressure, axial pressure, and confining pressure of the samples in autoclave in real time. Figure 2 shows the photos of the servo-controlled triaxial experimental system (Fig. 2a) and the rock sample that has been installed with two displacement gauges (Fig. 2b).

Experimental method

The composition of hydrate sediment in different marine areas is quite different (Zhu et al. 2011). Take the hydrate samples obtained in the South China Sea for example, analysis of hydrate samples indicates that most of the hydrate reservoirs found in the South China Sea are unconsolidated sediment. The aim of the experiments is to analyze the stress sensitivity of unconsolidated muddy sandstone reservoirs that store natural gas hydrates. Therefore, the test samples used in this study are artificial samples with no hydrate, and the ratio of sand and clay in the rock sample is 1:3. Seven standard diameter samples were prepared and used for stress sensitivity experiment. The basic characteristics of rock samples are demonstrated in Table 1.

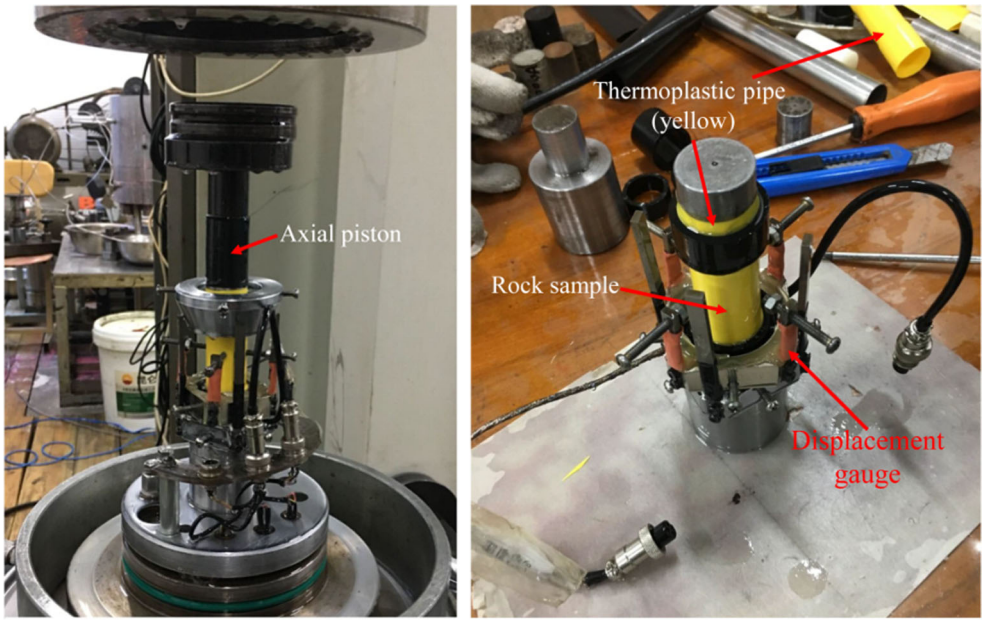

a Triaxial rock mechanics testing machine **b** Installation of core and deformation gauge

Fig. 2 Photos of the servo-controlled triaxial experimental system and the placed sample

Table 1 Basic characteristics of rock samples

No.	Length (mm)	Diameter (mm)	Density (kg/m^3)	Effective stress (MPa)
1	53.20	24.60	2030	0.0
2	51.00	24.60	2014	5.0
3	53.23	24.80	2020	10.0
4	52.80	24.70	1985	15.0
5	53.00	24.50	2025	20.0
6	52.22	24.50	2018	25.0
7	52.41	25.10	2020	30.0

In order to study the stress sensitivity of the unconsolidated sandstone, the experimental method of fixing the pore pressure and adjusting the confining pressure is adopted. The stress sensitivity experiment of unconsolidated sandstone is performed in the following two steps:

(1) Preparation and placement of rock samples. Mix the sand and soil into the mold and use the triaxial test machine to compact the sample. Thereafter, the thermoplastic tube is placed around the sample to prevent the hydraulic oil from entering the sample, and the displacement gauges are then placed around the core to measure axial and radial deformations.
(2) Determination of physical parameters. Keep the confining pressure and pore pressure constant and slowly loaded the axial pressure at a rate of 0.1 KN/s until the sample is damaged; both the stress-strain curve and the permeability curve can be obtained simultaneously during the loading process. During the whole experiment, the physical parameters of the rock samples were measured over the effective stress range from 0 to 30 MPa.

Experimental results and analysis

After obtaining the physical parameters, for the convenience of analysis, dimensionless treatment of the experimental results is adopted to study the stress sensitivity of the reservoir bearing sediments. The dimensionless result is defined as the ratio of the experiment value to the initial value. The stress sensitivity analysis of four physical parameters (Poisson's ratio, porosity, permeability, and elastic modulus) is conducted in this study. When the effective stress is gradually increased from 0 to 30 MPa, the relationships between the physical parameters (dimensionless Poisson's ratio, dimensionless permeability, dimensionless porosity, and dimensionless elastic modulus) of the reservoir and the mean effective stress are obtained by a series of experiments. Figure 3 shows the dimensionless results obtained experimentally.

As can be seen in Fig. 3a, Poisson's ratio of the reservoir rocks increases slightly with the increase of average effective stress. The binomial fitting form between Poisson's ratio and mean effective stress has higher fitting accuracy, and the general form can be expressed using the following equation:

$$v_{dim} = v_{exp}/v_{ini} = a{\cdot}\sigma^2 + b{\cdot}\sigma + c \quad (1)$$

where the variable v represents the Poisson's ratio; σ is the mean effective stress in MPa, and it can be calculated by $\sigma = (\sigma_1 + \sigma_2 + \sigma_3)/3$, where σ_1, σ_2, and σ_3 are the principal stresses; subscript *dim*, *exp*, and *ini* are the dimensionless data, the experimental data, and the initial experimental data, respectively; and a, b, and c are the regression coefficients for experimental data (the regression coefficients of the experimental data in this study are $a = -0.0002$, $b = 0.0139$, and $c = 0.9697$ ($R^2 = 0.6911$)).

Figure 3b shows the experimental results and the fitting curve of dimensionless permeability. The permeability of reservoir rock decreases significantly with the increase in the mean effective stress when the effective stress is less than 20 MPa, but the curve tends to be stable when the effective stress exceeds 20 MPa. As with the dimensionless Poisson's ratio, the fitting binomial formula with the correlation coefficient of $R^2 = 0.9801$ is well consistent with the experimental data. The general form of stress sensitivity fitting curves for dimensionless permeability can be described as follows:

$$K_{dim} = K_{exp}/K_{ini} = d{\cdot}\sigma^2 + e{\cdot}\sigma + f \quad (2)$$

where K is the permeability of reservoir rock and d, e, and f are the regression coefficients for experimental results, which are 0.0009, −0.0495, and 0.9745, respectively, in this study.

Within the range of effective stress studied in the experiment, the dimensionless porosity of reservoir rock ϕ_{dim} decreases with the increase of mean effective stress σ, as shown in Fig. 3c. It is understandable that as the effective stress gradually increases, the effective porosity within the rock

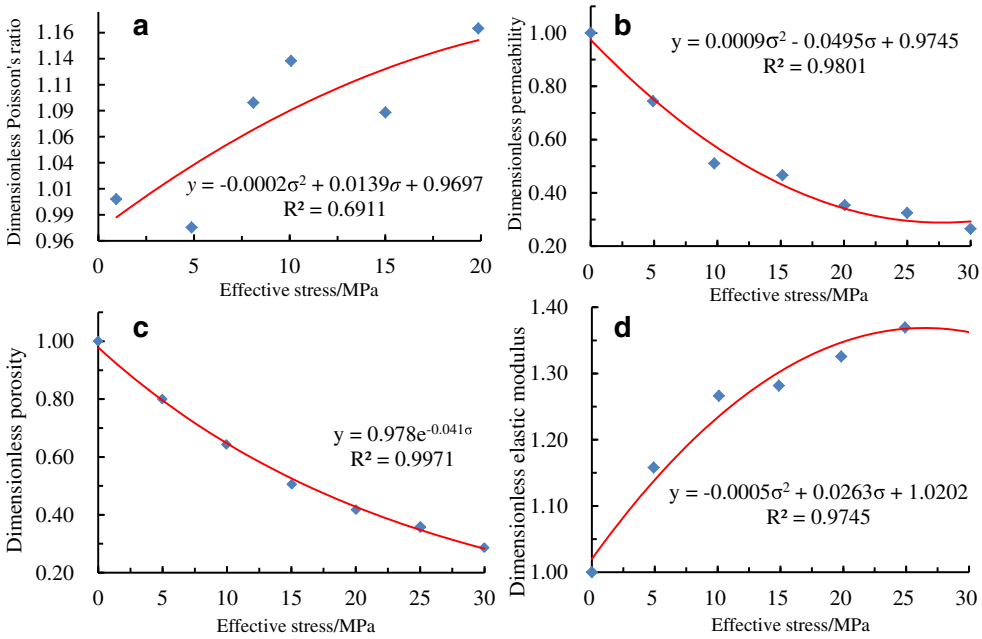

Fig. 3 Dimensionless results of the stress sensitivity experiment. **a** Dimensionless Poisson's ratio. **b** Dimensionless permeability. **c** Dimensionless porosity. **d** Dimensionless elastic modulus

sample is compressed, and the reservoir rock will be further compacted correspondingly, resulting in a gradual decrease in porosity and permeability. In fact, an exponential function with a natural constant as the base can be used to describe the relationship between ϕ_{dim} and σ, which is expressed by the following formula:

$$\phi_{dim} = \phi_{exp}/\phi_{ini} = g{\cdot}\exp(h{\cdot}\sigma) \tag{3}$$

where g and h are the coefficient and exponent of the fitting formula, respectively. In the study, g and h are 0.978 and −0.041 when the correlation coefficient R^2 is equal to 0.9971.

The dimensionless elastic modulus of the reservoir rock shows the similar variation trend with the dimensionless Poisson's ratio, and it can also be expressed by a binomial function with a correlation coefficient R^2 of 0.9745; the general form of the fitting function is shown as the following equation:

$$E_{dim} = E_{exp}/E_{ini} = i{\cdot}\sigma^2 + j{\cdot}\sigma + k \tag{4}$$

where i, j, and k are the coefficients of the fitting function, and they are −0.0005, 0.0263, and 1.0202 in this experiment, respectively.

Comprehensive modeling for the physical parameters of hydrate reservoir

As stated above, some defects still exist in the modeling for the physical properties of hydrate reservoirs, although some progress has been made (Masuda et al. 1997; Kambiz and Goodarz 2007; Freij-Ayoub et al. 2007). Among them, failure to take into account the stress sensitivity is on the top of the list. Therefore, a comprehensive model considering the stress sensitivity is established and verified by analyzing of wellbore stability in hydrate sediments.

Comprehensive model for pore characteristics

Li et al. (2014) established a model for the relationship between the relative permeability of hydrate bearing sediments in the South China Sea and hydrate saturation using the nuclear magnetic resonance measurements. In this model, the relative permeability of the hydrate reservoir decreases exponentially with the hydrate saturation, which is shown as the following equation:

$$K_{rel} = K(S_h)/K_0 = (1{-}S_h)^{7.9718} \tag{5}$$

where S_h is the hydrate saturation and K_{rel}, $K(S_h)$, and K_0 correspond to the relative permeability, permeability of hydrate reservoir, and the permeability of hydrate-free reservoir, respectively.

For conventional hydrate-free reservoirs, formation permeability can be assumed to be affected only by the mean effective stress σ, as shown in Eq. (1). However, for hydrate reservoirs, hydrate reservoir permeability is also a function of hydrate saturation S_h. Therefore, the comprehensive model of hydrate reservoir permeability (Eq. (6)) is obtained by substituting Eq. (5) into Eq. (1).

$$K(S_h,\sigma) = K_0{\cdot}\left(d{\cdot}\sigma^2 + e{\cdot}\sigma + f\right){\cdot}(1{-}S_h)^{7.9718} \tag{6}$$

Similarly, the effective porosity of hydrate reservoir $\phi(S_h)$ is also affected by hydrate saturation, and the relationship between them is expressed as follows (Masuda et al. 1997):

$$\phi(S_h) = \phi_0 \cdot (1 - S_h) \tag{7}$$

where ϕ_0 is the porosity of hydrate-free reservoir.

Considering the effect of hydrate dissociation (Eq. (7)) and stress sensitivity (Eq. (3)) on the porosity of hydrate reservoirs, a comprehensive model of hydrate reservoir porosity is obtained, which can be given by

$$\phi(S_h, \sigma) = \phi_0 \cdot (1 - S_h) \cdot (g \cdot \exp(h \cdot \sigma)) \tag{8}$$

Comprehensive model for elastic parameters

Assume that the Poisson's ratio of hydrate reservoir does not vary with the hydrate dissociation (Klar and Soga 2005; Masui et al. 2005). That is, the Poisson's ratio of the hydrate reservoir in the comprehensive model is only a single-variable function of the mean effective stress, so it can be obtained by Eq. (1) and given as the following formula:

$$v(\sigma) = v_0 \cdot \left(a \cdot \sigma^2 + b \cdot \sigma + c\right) \tag{9}$$

where v_0 is the Poisson's ratio before hydrate dissociation.

Kim (2016) obtained the change of elastic modulus during hydrate dissociation by experiment, which can be written as the following formula:

$$E = E_0 \cdot (1 + 13.25 \cdot S_h) \tag{10}$$

As with the above process, the comprehensive model of elastic modulus in hydrate reservoir can be obtained by combining Eqs. (4) and (10), which is shown as the following equation:

$$E(S_h, \sigma) = E_0 \cdot (1 + 13.25 \cdot S_h) \cdot \left(i \cdot \sigma^2 + j \cdot \sigma + k\right) \tag{11}$$

where E_0 is the elastic modulus of hydrate-free sediment.

Comprehensive model for strength parameters

Hydrate dissociation produces extra pore space and thus damages the cementation between the matrix particles within the formation. Freij-Ayoub et al. (2007) established a linear model of cohesion and porosity during hydrate dissociation, as follows:

$$C(S_h, \sigma) = C_0 \cdot (1 - 1.2 \cdot (\phi - \phi_0)) \tag{12}$$

where C and C_0 are the new and initial cohesion of hydrate sediments. Besides, with respect to the change of the internal friction angle during the hydrate dissociation, Shi (2009) established the directional relationship between the internal friction angle $\theta(S_h)$ and the cohesion in the study of the wellbore stability, which is shown as the following equation:

$$\theta(S_h, \sigma) = 20 + 2.564 \cdot lg\left[(59.83 - 1.785C)^2 + \sqrt{60.83 - 1.785C}\right] \tag{13}$$

Although the hydrate saturation S_h and the effective stress σ are not present in Eqs. (12) and (13), the porosity $\phi(S_h)$ is a function of the hydrate saturation and the effective stress (as shown in Eq. (8)). Thus, Eqs. (12) and (13) can indirectly indicate the comprehensive model for strength parameters of hydrate sediment.

As for the dilation angle ψ, it is assumed that it is just relevant to the hydrate saturation, and has nothing to with stresses. The relationship between dilation angle and hydrate saturation is expressed by the following equation (Ng et al. 2008):

$$Sin(\psi) = 0.05 + 0.5 S_h \tag{14}$$

Implementation of comprehensive model

Basic of wellbore instability

Wellbore instability is a common accident in the process of drilling, mainly attributed to the replacement of rock within borehole with drilling mud during the drilling operation, which brings about stress redistribution and concentration within the surrounding rock and disturbs its stability. The borehole will be destroyed when the stresses of the surrounding rock exceed the rock strength (Cheng 2015). Modeling of wellbore stability during methane gas hydrate development is a complex undertaking, which consists of many different physical processes (i.e., heat transfer, invasion of drilling fluid into the hydrate formation, hydrate dissociation, and wellbore instability). Different wellbore structures are suitable for different purposes (Merey 2016). In general, hydrate exploration usually adopts riserless drilling (as illustrated in Fig. 4a), whereas drilling with riser are generally conducted for hydrate development (Fig. 4b). Considering that the drilled borehole is still used for the subsequent development of the hydrate, the offshore drilling with riser is adopted (Merey 2016), and the configuration of hydrate drilling system is illustrated as Fig. 4 (Qiu et al. 2014). There are mainly three components within the wellbore stability system: casing, drill pipe, and the reservoir. Due to complicated thermo-hydro-mechanical interactions within hydrate reservoir, a finite element model is created by ABAQUS software for simulating the non-liner behavior of borehole.

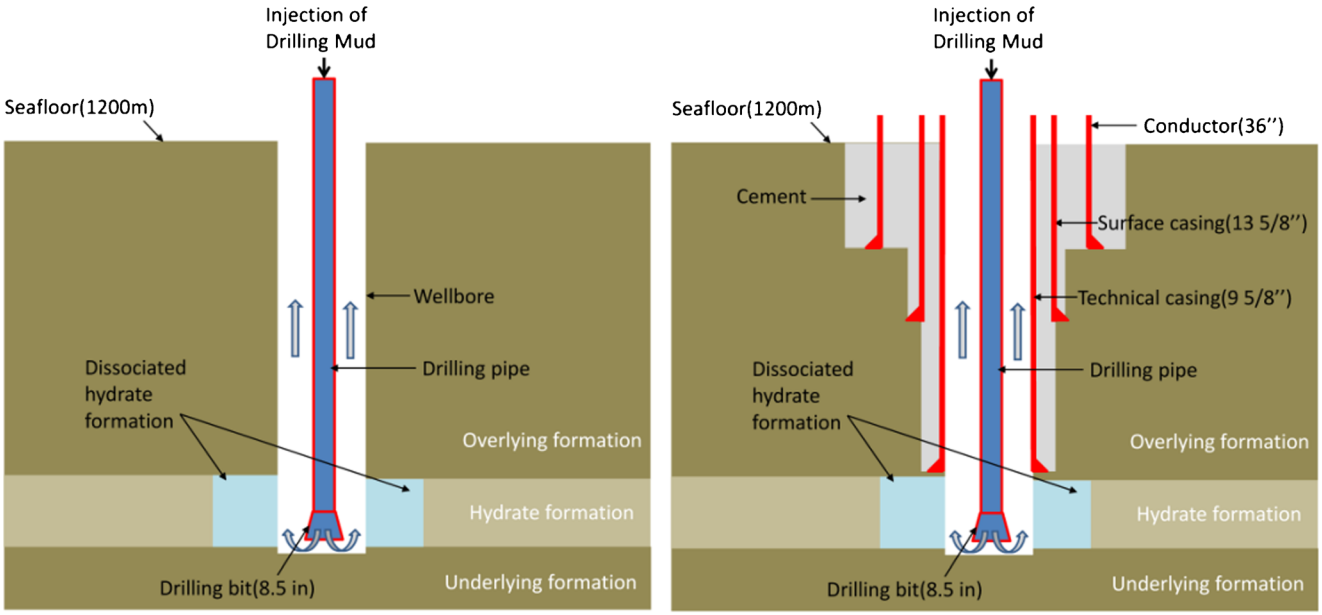

Fig. 4 Configuration diagram of hydrate drilling system

Hydrate dissociation and coupling mechanism

The stability of natural gas hydrate is mainly determined by factors of temperature, pressure, gas composition, and pore fluid salinity (Wu et al. 2007). According to results of geophysical exploration for hydrate reservoirs in the South China Sea, the composition of hydrocarbons in hydrate of the South China Sea is mainly methane (to be exact, between 96 and 100%); ethane and propane only occupy a small share (Wu et al. 2007, 2011; Li et al. 2010). In this case, the *P-T* relationship of pure methane hydrate in seawater is given as the following equation (Sun et al. 2011):

$$P_d = 9 \times 10^{-14} e^{0.1136 T_d} \quad (15)$$

where P_d is the pressure in MPa and t_d is the temperature in K at any depth below the seafloor.

At a given pressure, the hydrate phase equilibrium temperature will decrease correspondingly when the appropriate hydrate inhibitor is added. The reduced amplitude can be calculated by (Hammerschmidt 1939)

$$\Delta T = 2335 \times C/M(100\text{-}C) \quad (16)$$

where ΔT is the temperature depression caused by inhibitor, °C; C is the inhibitor concentration, wt%; and M is the molecular weight of inhibitor.

Hydrate exists in solid form at several hundred meters below the seafloor, but it gradually dissociates when the temperature rises above equilibrium temperature or pressure falls below phase equilibrium pressure (Klar and Soga 2005; Tréhu et al. 2006; Merey 2016). Based on hydrate phase equilibrium conditions and the established comprehensive model, two field variables are defined firstly to realize the hydrate dissociation effect and the stress sensitivity effect, respectively. By writing the USDFLD subroutine, the temperature, pore pressure, and stresses of every integration point within the hydrate formation are imported into the simulation program to implement the established comprehensive model.

Figure 5 shows the computational algorithm used for predicting wellbore stability while drilling in hydrate formation. The order for the sequential coupling of the heat transfer-seepage-deformation multi-physics simulation can be described as follows: (1) heat transfer analysis is carried out firstly to obtain the spatial distribution of temperature on each node; (2) then, the temperature result obtained in the previous step is imported into the coupled solid-fluid model for analysis; and (3) with the help of the USDFLD subroutine, both hydrate dissociation and thermal-fluid-solid coupling analysis can be performed. Consequently, the wellbore stability while drilling in the hydrate formation can be analyzed. Nevertheless, it should be noted that the model size and element size should be consistent in heat transfer analysis and the subsequent thermo-hydro-mechanical coupling analysis, and the only difference is the element type, which will be described in detail in the following sections.

Geomechanical modeling for analysis of wellbore stability

Developing a finite element model for simulating wellbore stability mainly contains the following steps: describing the model geometry, boundary and initial condition definition, and the material property definition.

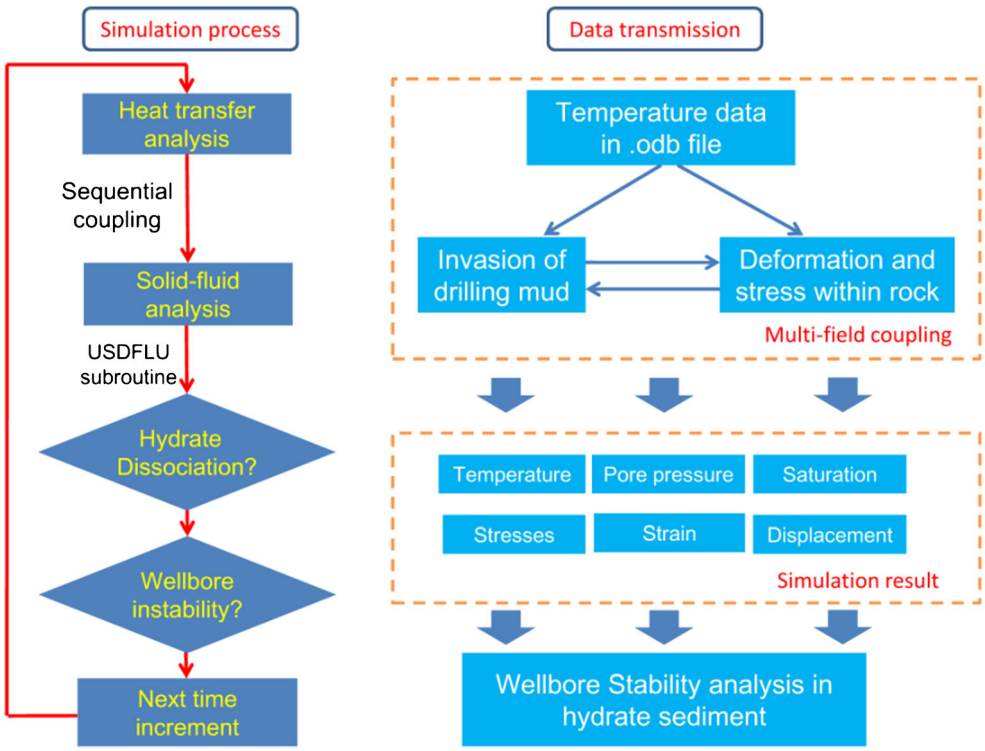

Fig. 5 Sequential coupling process of wellbore stability analysis during drilling in hydrate formation

Finite element modeling and material

The target well is a vertical well for hydrate development in the Shenhu area of the South China Sea, and the measured seafloor depth is about 1230 m (Wang et al. 2011). Owing to the serious lack of description for methane hydrate development wells drilled in the South China Sea, borehole structure of target well should refer to the wells in similar sea area; the size of different casings used for simulation are described as Fig. 4b (Qiu et al. 2014).

The site SH2, which is one of the earliest sites for hydrate exploration in the South China Sea by the Chinese Geological Survey in 2007, is taken as the example to analyze the wellbore stability. The hydrate layer is located at the depth between 195 and 220 m (Xiao et al. 2013; Yang et al. 2008). The finite element model in Fig. 6 consists of only one component: the formation. To avoid the influence of far field boundary effect on simulation results, the dimension of the finite element model is 25 m in both the X (lateral) and Y (vertical) directions, and the wellbore size is set to be 8.5 in. The red lines of AB and CD in Fig. 6 are two paths located in X and Y directions along the radial direction, respectively.

To improve the quality of meshing, partitioning the model into separate parts is necessary. To be exact, the finite element model is divided into two parts, the near-wellbore region and the far-field region. The elements within the near-wellbore region are uniform, but the elements inside the far-field region change along the radius in a certain proportion; sizes of elements close to the near-wellbore are set to be five times as larger as that of elements on the boundary. After meshing, there are 3840 DC2D4 or CPE4P elements within the whole model. Among them, the DC2D4 elements are heat transfer elements for simulating the heat transfer process, and the CPE4P elements are pore fluid/stress element for carrying out the fluid-solid coupling simulation. In addition, the characteristics of hydrate formation for the simulation model are listed in Table 2.

Boundary conditions and initial conditions

Just as shown in Fig. 5, the simulation adopts the one-way coupling technique, and it can be divided into two phases, i.e., heat transfer analysis and solid-fluid coupling analysis. Normal displacement of the wellbore and the outer boundary are fixed during the whole simulation. Besides, the wellbore during the heat transfer simulation is set to be the temperature boundary, but it needs to be converted to the pore pressure boundary in the solid-fluid coupling analysis. The drilling conditions used in this paper determine that the numerical model simulates the over-balanced drilling process, which can ensure that the hydrate dissociation is minimized.

In terms of the variation of formation temperature with depth, Wang et al. (2011) have fitted the field temperature measured at the SH2 site, and gave the curve of temperature versus depth.

$$T = 0.0456d + 5.6723 \quad (17)$$

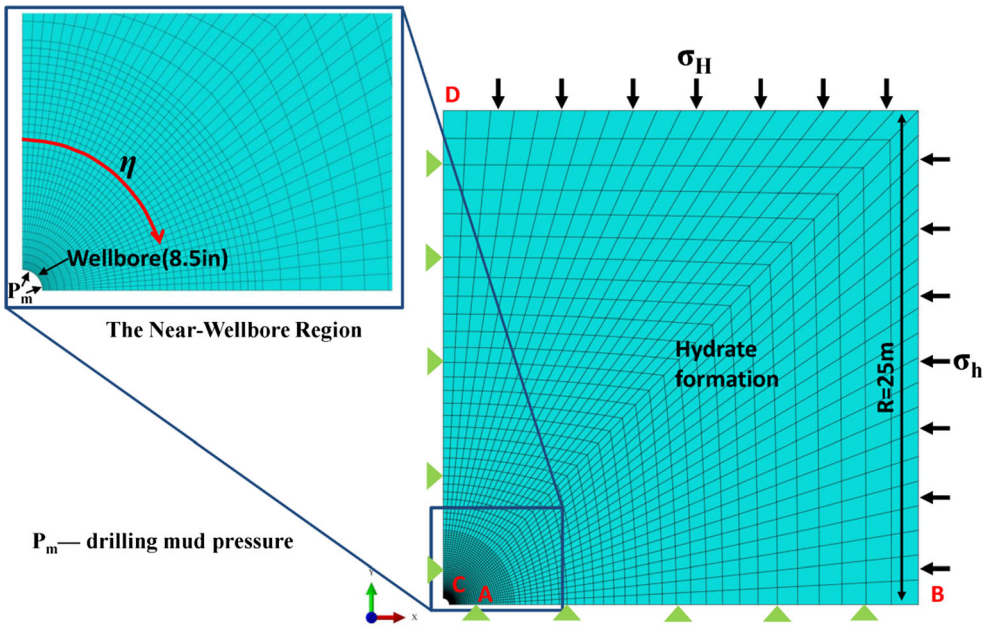

Fig. 6 The finite element model and mesh

where the parameter T is the temperature in °C at certain depth of d (mbsf) and d is determined to be 200 m. Assuming that the pore fluid in sediment is considered to be interconnected with seawater, and then the hydrostatic pore pressure can be calculated from the depth and the average seawater density (Ning et al. 2013a; Ning et al. 2013b).

$$P_p = \rho_{sewat} g(d + H) \tag{18}$$

where the seawater density ρ_{sewat} is 1.03 g/cm^3 and H is the depth of seawater (m).

Porosity of the formation also changes with depth; it can be expressed as Eq. (12) (Guo et al. 2011), and the void ratio e can be calculated by $e = \phi/(1 - \phi)$.

$$\phi = (-7.4366 \times \ln(d) + 85.3829)\% \tag{19}$$

Initial conditions should be defined to carry out the simulation, which consists of initial pore fluid saturation, initial void ratio, initial temperature, initial pore pressure, and initial geostress field. The initial conditions are listed in Table 3. Figure 7 indicates the practical conditions of hydrate formation in Shenhu area and the phase equilibrium conditions. As can be observed from the curve in the figure, hydrate in formation is in the steady state, and the temperature and pressure conditions of the drilling mud may lead to the dissociation of the hydrate. Then, the wellbore may lose stability due to hydrate dissociation.

The mechanical properties of hydrate formation change with the hydrate dissociation and stresses within the formation, which will, in turn, significantly affect both the exploitation of hydrate and wellbore stability. Mostly, mechanical parameters of the hydrate formation are considered to be related

Table 2 Physical parameters of simulation model and the drilling conditions

Parameter	Value	Unit	Reference
Density, ρ	2000	kg/m^3	Liu et al. (2017)
Initial Young's modulus, E_0	625	MPa	Ng et al. (2008)
Initial dilation angle, ψ	17.46	°	
Poisson's ratio, v_0	0.45	–	Freij-Ayoub et al. (2007)
Friction angle, ϵ	35	°	
Initial cohesion, C_0	1250	KPa	Ng et al. (2008)
Thermal conductivity, λ	1.5	W/(m K)	Wan et al. (2016)
Specific heat capacity, C_{sh}	1362	J/(kg K)	Zhao (2010)
Initial permeability, k_0	10	mD	Su et al. (2011)
Initial porosity, ϕ_0	45.98	%	Guo et al. (2011)
Initial hydrate saturation, S_{h0}	47	%	Su et al. (2011)
Drilling mud pressure, P_m	15.5	MPa	
Drilling mud temperature, T_m	17.79	°C	
Drilling time, t_d	3.00	h	

Table 3 Initial conditions in the model

Initial conditions	Value	Unit	Reference
Saturation	1	–	–
Void ratio	0.8512	–	Equation (19)
Pore pressure	14.64	MPa	Equation (18)
Vertical effective stress, σ_V	1.1	MPa	Cha et al. (2016)
Maximum horizontal stress, σ_H (Y)	0.6	MPa	–
Minimum horizontal stress, σ_h (X)	0.8	MPa	–
Temperature	14.79	°C	Equation (17)

only to the hydrate saturation (Ng et al. 2008; Konno et al. 2010). However, the effective stress of the hydrate formation during the hydrate dissociation process is another factor contributing to the change of mechanical parameters; the implementation of the comprehensive model has been described above.

Validation of the comprehensive model

Based on the numerical model and theory mentioned above, a quarter of the two-dimensional finite element model is established, considering the symmetry of both the formation and the wellbore. A series of simulations have been performed to verify the comprehensive model and analyze the impact of hydrate dissociation caused by drilling mud invasion during hydrate drilling phase on wellbore stability.

Hydrate dissociation during drilling operation

Based on the basic assumption that reservoir fluid flow and rock deformation do not affect the heat transfer process, Fig. 8 shows the temperature distribution along AB at different times. As illustrated in Fig. 8, the temperature front moves forward gradually within the near wellbore region over time. It can be clearly found that heat conduction is a very slow process, and as the drilling time passes, the advancing speed of the temperature front becomes slower and slower. When the drilling mud that with the constant temperature of 17.79 °C is in contact with the hydrate formation that with the initial temperature of 14.79 °C for 3 h; that is, when the hydrate formation is drilled for 3 h, the temperature front goes deep to a depth of 0.26 m from wellbore. The result confirms the predecessors' conclusions that it is not a wise choice to develop hydrates just relying on the hot fluid heating in wellbore (Li et al. 2011; Su et al. 2010; Moridis and Reagan 2007). Additionally, it is still an important issue and challenge to ensure that the drilling fluid is at a lower temperature during the drilling phase.

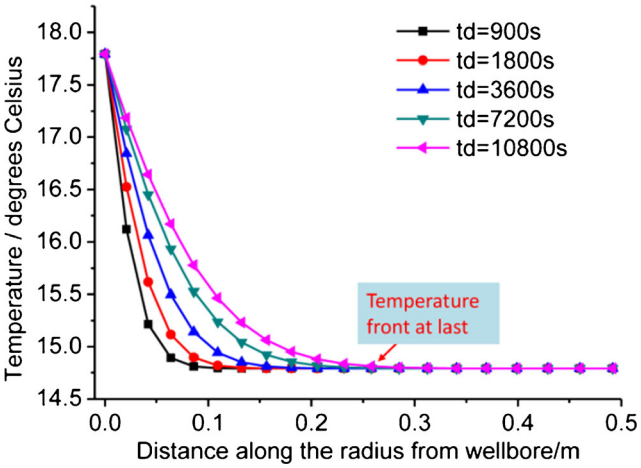

Fig. 8 Temperature distribution within the near-wellbore region along the path of AB at different times

During the overbalanced drilling, the invasion of high-pressure drilling mud prevents the hydrate within the reservoir from dissociation, whereas the high-temperature drilling mud will boost its dissociation. Figure 9 shows the spatial

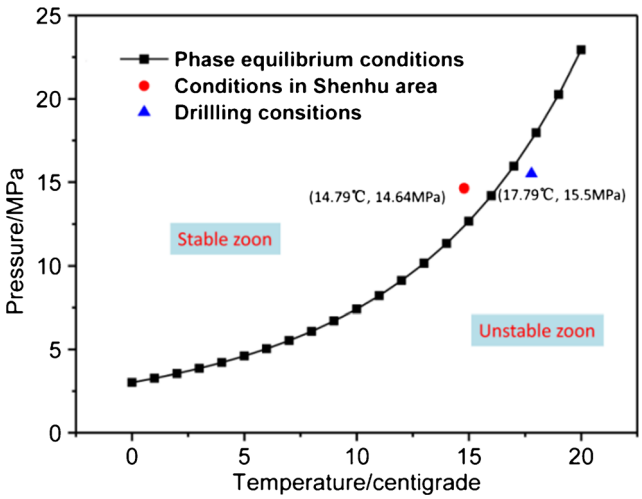

Fig. 7 Temperature and pressure conditions of drilling operation and the phase equilibrium conditions

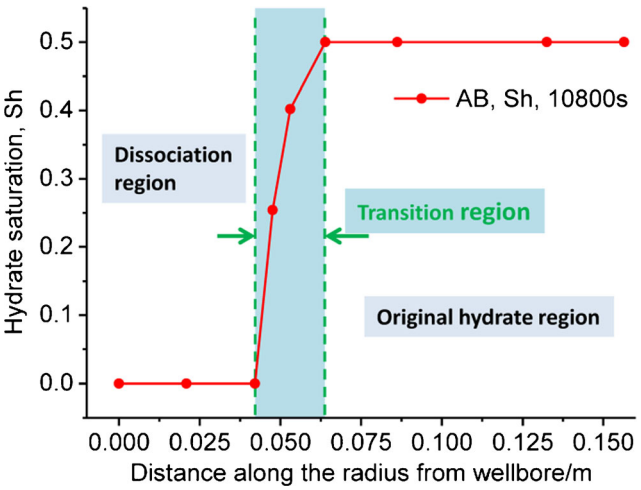

Fig. 9 Hydrate saturation along the path of AB or CD at the last of the drilling operation

distribution of hydrate saturation at the end of the drilling phase. As illustrated in the figure, continuing drilling for 3 h in hydrate formation under the drilling conditions given in this paper resulted in a hydrate dissociation of about 6 cm in thickness. However, the hydrate dissociation process does not occur instantaneously, and therefore, there is a transition region between the original hydrate region and the hydrate dissociation region. It can be seen from Fig. 9 that the thickness of transition region is about 2 cm under the drilling conditions in this paper.

Effect of stress sensitivity on pore pressure propagation

Figure 10 shows the results of pore pressure along the radius direction whether the stress sensitivity is considered or not at different circulation times. It is observed that the pore pressure travels faster than the heat of the drilling fluid during overbalanced drilling operation in hydrate formation. At the end of the drilling phase, pore pressure propagated to the place that is about 20 m away from the borehole (Fig. 10f), which is up to 77 times the heat transfer distance (i.e., 0.26 m; see in Fig. 8). Logically speaking, the seepage in the porous media mainly depends on the permeability coefficient of the formation, and the propagation of pore pressure in homogeneous and isotropic formation should be the same in all directions if the stress sensitivity has not been taken into account. Nevertheless, the permeability coefficient is relevant to the hydrate saturation S_h and the stresses in every node within the formation. According to Fig. 3b and Eq. (2), the permeability coefficient decreases gradually with the increase of the mean effective stress.

As can be seen from every subgraph in Fig. 10, at any time, the pore pressure at any node for the model in which the mean effective stress is considered is generally greater than that of the conventional model (in which the effect of mean effective stress is not taken into account). This difference is shown in Fig. 10 as the separation of the pore pressure curves for the two models. Moreover, as the drilling operation continues, the pore pressure gradually propagates from the borehole to the distant formation, and the separation of the pore pressure curves for the two models is more and more obvious. This is because, when the physical properties of the hydrate formation are modeled, if the effect of the mean effective stress on the permeability coefficient is taken into account, the decrease in the permeability coefficient hinders the invasion of drilling fluid and its seepage in the formation.

Effect of stress sensitivity on the equivalent plastic strain

Equivalent plastic strain is one of the parameters that can be used to evaluate whether the wellbore will undergo deformation and instability. The collapse and instability of wellbore always occur at the Gaussian integral node where the equivalent plastic strain is largest (Huang 2016). That is, the wellbore instability may occur at any location near the wellbore region where the plastic yield is presented. Because the drilling process will only lead to a small yield area, Fig. 11 indicates the equivalent plastic strain of the near-wellbore at different times during the hydrate drilling process.

As can be seen from Fig. 11, under the effect of nonuniform horizontal stresses, the stress of rock around the wellbore in the direction of the minimum horizontal stress is the most concentrated, and the surrounding rock in this direction is most likely to be unstable. Consequently, as can be seen in Fig. 11, the maximum equivalent plastic strain always exists in the direction of minimum principal stress (X axis direction). Besides, the maximum plastic strain increases as the drilling operation continues. At the end of the drilling phase, the maximum equivalent plastic strain for the model in which the stress sensitivity is considered has reached 0.01447.

In order to determine the influence of mean effective stress on the physical parameters of hydrate sediments, the relative error δ is defined to describe this difference, which is performed by the Eq. (20).

$$\delta = \frac{|PEEQ_{no-stress} - PEEQ_{stress}|}{PEEQ_{stress}} \times 100\% \tag{20}$$

where $PEEQ_{no\ stress}$ and $PEEQ_{stress}$ are the maximum plastic strain of the comprehensive model that considers the stress sensitivity and that of the traditional model that does not consider the effect of stress, respectively.

Table 4 displays the comparison results of the maximum equivalent plastic strain between two different models at different times. From Table 4, we can see that the relative errors of the equivalent plastic strain during the whole drilling operation are all greater than 10%. In addition, the maximum equivalent plastic strains of the established comprehensive model at different times are always greater than that of the traditional model. This is because that when the stress sensitivity is considered, the decrease in permeability hinders the invasion of the drilling fluid into the formation, which reduces the dissociation of natural gas hydrate and thus results in a smaller equivalent plastic strain. Consequently, we can draw the conclusion that the accuracy of wellbore stability evaluation will be seriously restricted if the influence of stress on formation physical parameters is not taken into account.

Effect of stress sensitivity on wellbore deformation

Borehole size is a direct parameter describing the borehole stability. Figure 12 shows radial deformation of borehole at different times during drilling and the comparison of relative errors of radial deformation between two models. In order to better show the effect of hydrate dissociation on borehole

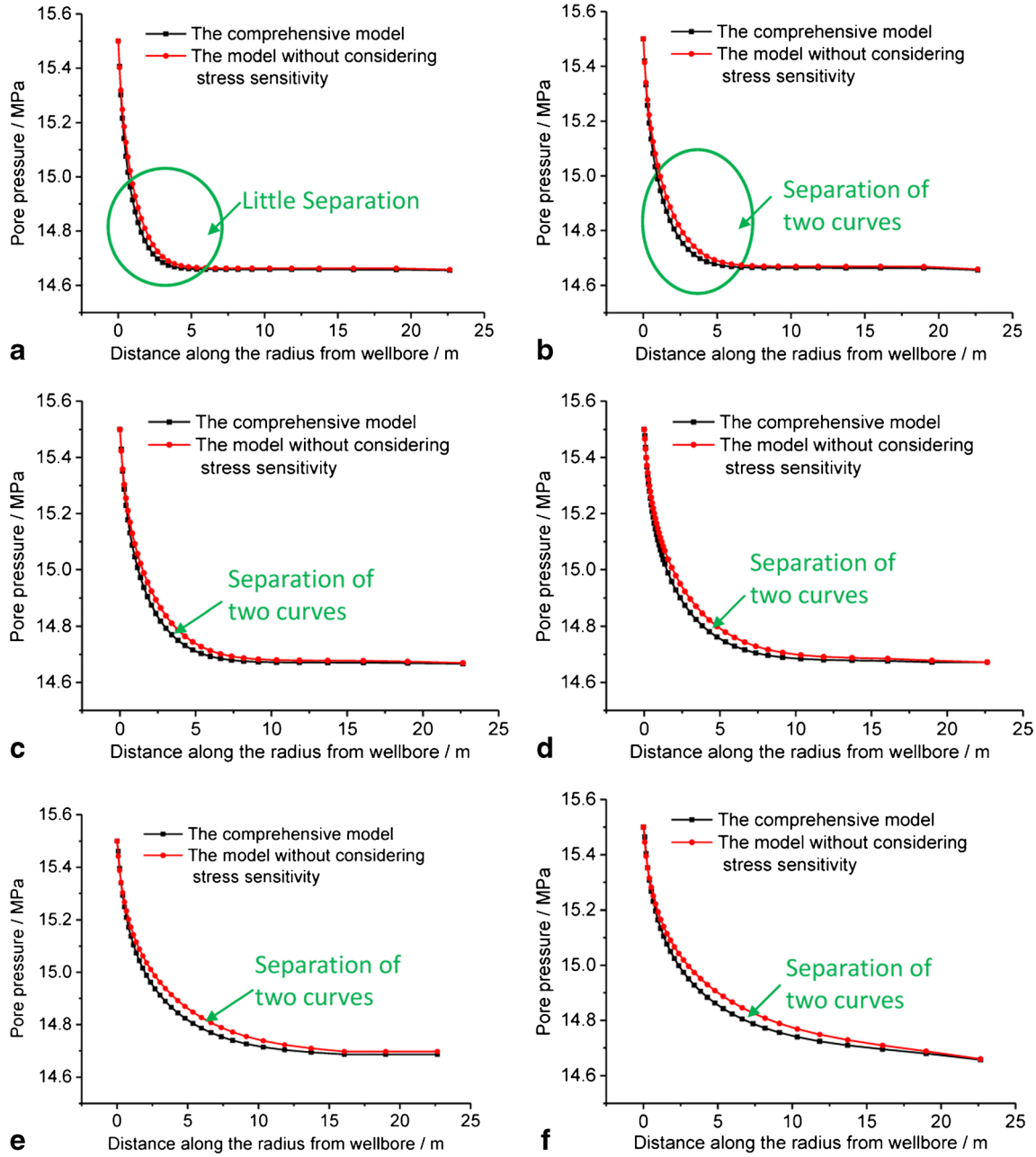

Fig. 10 The distribution of pore pressure along the radius direction (take AB for example) at different circulation times. **a** $t_d = 500$ s. **b** $t_d = 1000$s. **c** $t_d = 2000$s. **d** $t_d = 3600$ s. **e** $t_d = 7200$ s. **f** $t_d = 10{,}800$ s

deformation when stress sensitivity is considered, the deformation curves at different times are divided into two subgraphs. From Fig. 12, it could be found that the largest wellbore deformation caused by hydrate dissociation during drilling is always present in the direction of maximum horizontal principal stress (i.e., Y axis direction), but the severe stress concentration in the direction of the minimum horizontal principal stress results in the maximum diameter enlargement of the wellbore in this direction.

Not only that a tiny gap exists between two deformation curves (black line and red line), which indicates that the stress sensitivity has certain influence on the simulation and evaluation of borehole stability. The blue lines are the relative error curves for wellbore radius, and the relative error varies greatly with angle η. Besides, the largest relative error of borehole deformation for the two parametric models increases as the drilling operation continues, and detailed statistics are given in Table 5. After drilling in hydrate formation for half an hour, the relative error is only 2.02%, whereas the relative error has reached 75.99% at the end of the drilling phase.

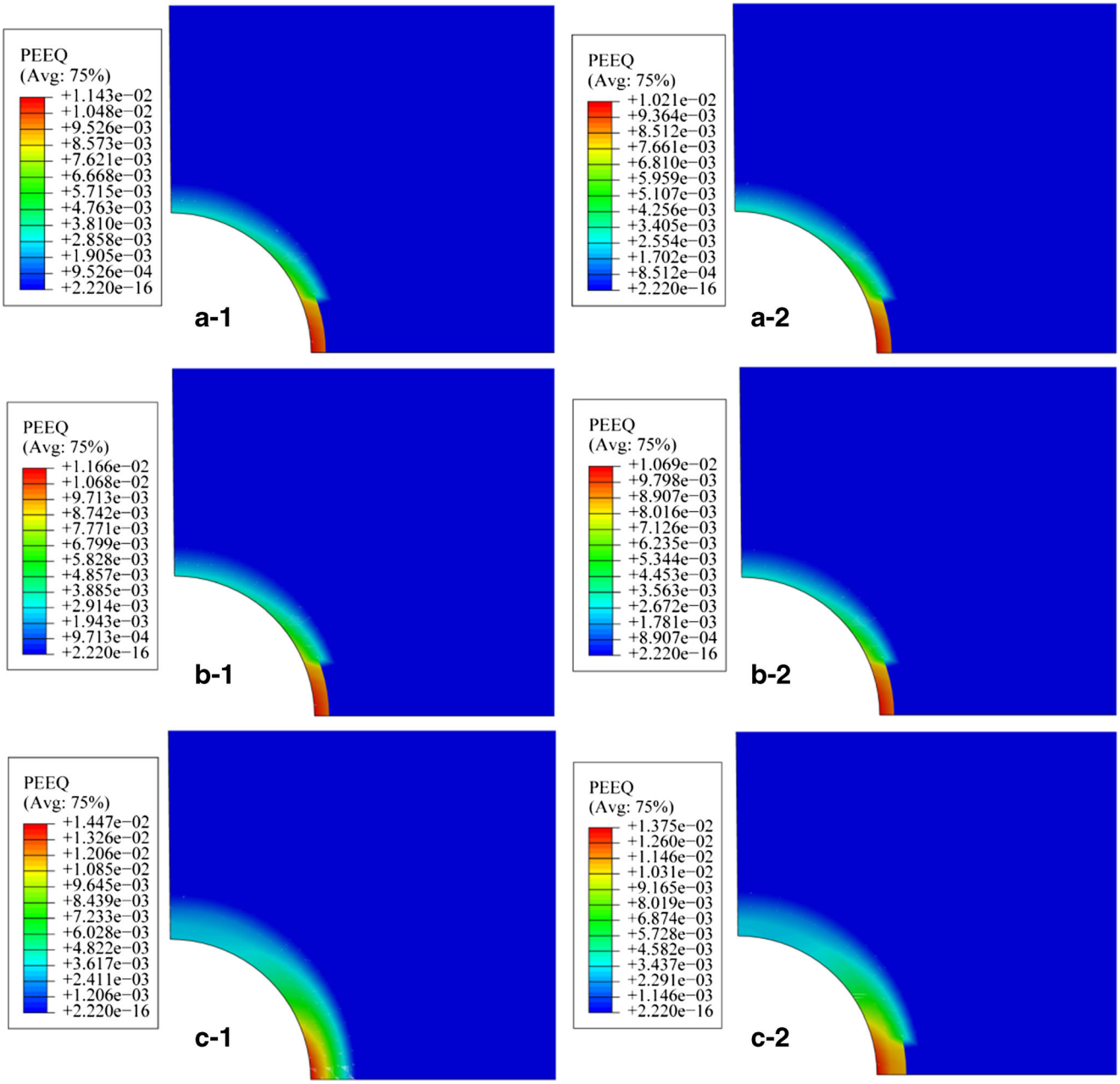

Fig. 11 Equivalent plastic strain of the formation within the near-wellbore region at different drilling times. **a** $t_d = 500$ s. **b** $t_d = 3600$ s. **c** $t_d = 10{,}800$ s. *1* The comprehensive model, *2* the model without considering the stress sensitivity

Table 4 Comparison of the maximum equivalent plastic strain between two models mentioned in this paper at different times

Time/s	1,800	3,600	7,200	10,800
The comprehensive model	0.01158	0.01167	0.01437	0.01447
The traditional model	0.01052	0.01069	0.01359	0.01375
Relative error δ/%	9.15	8.40	4.73	4.98

Conclusion

In this investigation, a series of experiments has been carried out to explore the effect of mean effective stress on properties of hydrate formation, and then, a comprehensive model for parameters of hydrate formation is established. Additionally, in order to verify the stress sensitivity of hydrate formation, a coupling thermo-hydro-mechanical numerical model has been established to analyze the wellbore stability while drilling in hydrate formation. Therefore, the conclusions obtained in this paper are approached as follows:

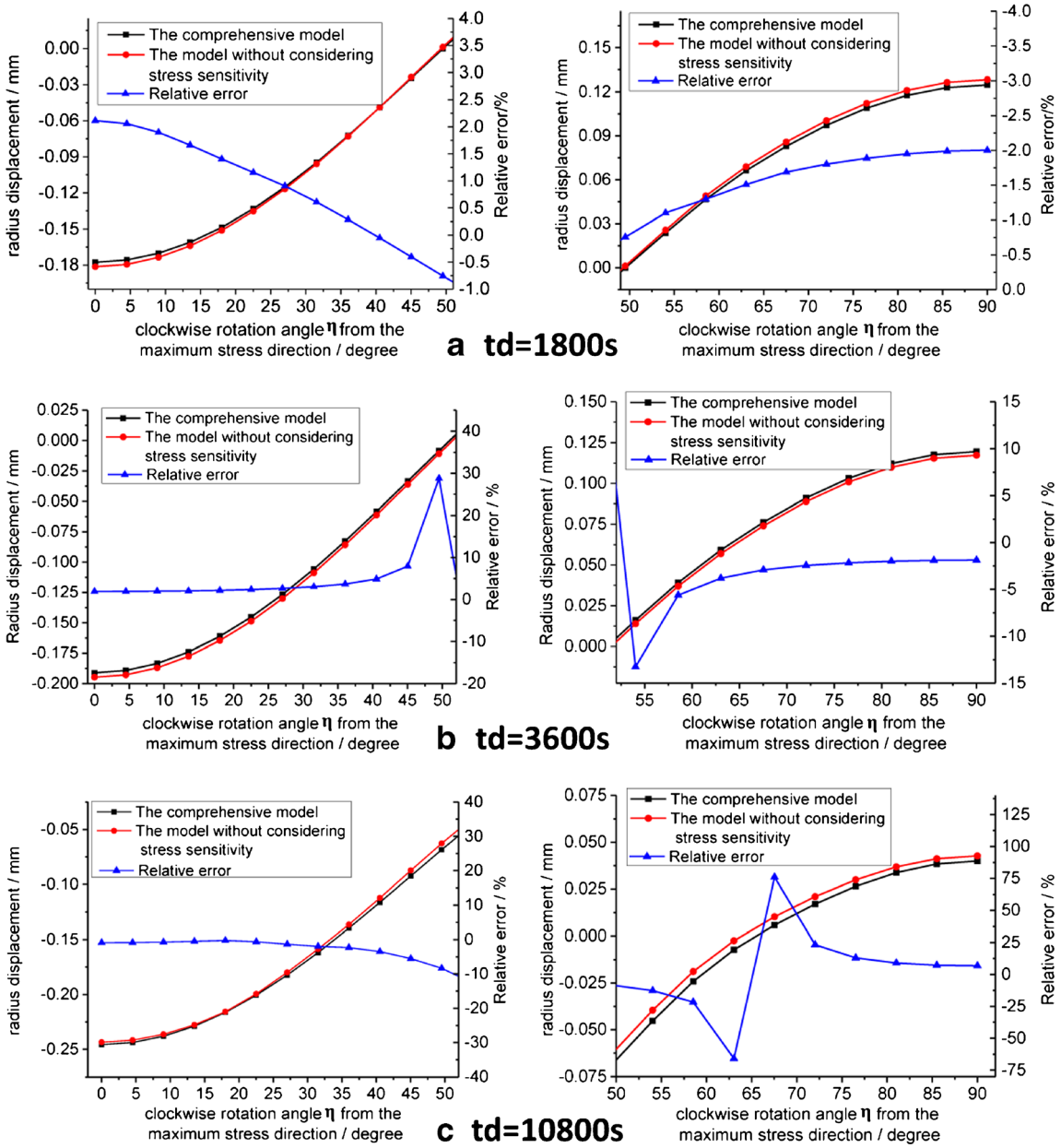

Fig. 12 Radial deformation of the borehole at different times during drilling phase and the relative error between the two models

1. Stress change caused by hydrate development has significant influence on the parameters of the unconsolidated sediment that forms the framework of hydrate reservoirs. Both dimensionless permeability and the dimensionless porosity decrease with the increase of the mean effective stress, but the dimensionless Poisson's ratio and the dimensionless elastic modulus show the opposite trend. Besides, the exponential fitting relationship between dimensionless porosity and mean effective stress can be well matched with the experimental data, while other dimensionless parameters can be fitted as binomial functions of the mean effective stress.
2. Based on the established comprehensive model and overbalanced drilling operation, drilling for 3 h lead to a decomposition range of about 6 cm thick in the hydrate formation, whereas the temperature front goes deep to a depth of 26 cm from wellbore. This is because that hydrate dissociation depends on two factors: pore pressure and temperature.

Table 5 Comparison of the maximum relative error between the borehole deformations for two models at different times

Time/s	1,800	3,600	7,200	10,800
The maximum relative error/%	2.02	28.86	73.20	75.99

3. In analyzing the wellbore stability while drilling in hydrate sediment, when the stress sensitivity is considered, the decrease in permeability caused by effective stress hinders the invasion of the drilling mud into the formation, which reduces the dissociation of natural gas hydrate and thus results in a smaller equivalent plastic strain.
4. Borehole size is a direct parameter to evaluate wellbore stability. By comparing the borehole size of the traditional model that without considering the influence of stress with that of the comprehensive model that considering the of stress sensitivity, it is found that the maximum relative error increases with the continuous drilling operation.

Acknowledgements This work was supported by Program for the Changjiang Scholars and Innovative Research Team in University (IRT_14R58) , the National Natural Science Foundation Project of China (51704311), the Fundamental Research Funds for the Central Universities (Grant No. 16CX06033A), National Key Research and Development Program (Grant No. 2016YFC0304005), the National Basic Research Program of China (973 Program) (Grant No. 2015CB251201), and Qingdao Science and Technology Project (Grant No. 15-9-1-55-jch).

References

Briaud JL, Chaouch A (1997) Hydrate melting in soil around hot conductor. J Geotech Geoenviron 123(7):645–653. https://doi.org/10.1061/(ASCE)1090-0241(1997)123:7(645).

Bybee K (2007) Gas production from oceanic class 2 hydrate accumulations. J Pet Technol 59(8):69–73

Cha Y, Yun T, Kim Y, Lee J, Kwon TH (2016) Geomechanical, hydraulic and thermal characteristics of deep oceanic sandy sediments recovered during the second ulleung basin gas hydrate expedition. Energies 9(10):775–797. https://doi.org/10.3390/en9100775

Cheng YF, Shen HC, Zhao YZ (2010) Study on fluid-solid coupling of physical variation of gas hydrate reservoirs during natural gas development. Acta Petrolei Sinoca 31(4):607–611

Cheng YF (2015) Oil and gas Engineering & Rock Mechanics. China University of Petroleum press, China.

Freij-Ayoub R, Tan C, Clennell B, Tohidi B, Yang J (2007) A wellbore stability model for hydrate bearing sediments. J Pet Sci Eng 57(1):209–220. https://doi.org/10.1016/j.petrol.2005.10.011

Gai X, Sánchez M (2017) A geomechanical model for gas hydrate-bearing sediments. J Environ Geol 4:143–156. https://doi.org/10.1680/jenge.15.00050

Guo Y, Qiao S, Lv W (2011) Vertical displacement of gas hydrate in Shenhu area of the South China Sea based on acoustic velocity. Marine Geology Frontiers 27(7):7–11

Hammerschmidt EG (1939) Preventing and removing gas hydrate formations in natural gas pipe line. Oil Gas J 37(52):66–72

Huang C (2016) A numerical investigation of wellbore stability problems using an elastoplastic model. Master's theses, Louisiana State University, USA.

Kambiz N, Goodarz A (2007) Computational modeling of methane hydrate dissociation in a sandstone core. Chem Eng Sci 62(22):6155–6177. https://doi.org/10.1016/j.ces.2007.06.038

Kim YM, Lee JS, Lee JY, Lee C (2012) Stress-dependant characteristics of deep marine sediments recovered from the Ulleung Basin, East Sea, Korea. World Congress on Advances in Civil, Environmental, and Materials Research, Seoul, Korea

Kim AR (2016) T-H-M Coupled Numerical Analysis of Gas Production from Methane Hydrate Deposits in the Ulleung Basin in Korea. PHD thesis, Korea Advanced Institute of Sci Technol, Republic of Korea.

Klar A, Soga K (2005) Coupled deformation-flow analysis for methane hydrate production by depressurized wells. International Biot Conference on Poromechanics, Oklahoma City, USA

Klar A, Soga K, Ng M (2010) Coupled deformation-flow analysis for methane hydrate extraction. Geotechnique 60(10):765–776

Konno Y, Masuda Y, Hariguchi Y, Kurihara M, Ouchi H (2010) Key factors for depressurization-induced gas production from oceanic methane hydrates. Energy Fuel 24(3):1736–1744. https://doi.org/10.1021/ef901115h

Kwon TH, Lee KR, Cho GC, Lee JY (2011) Geotechnical properties of deep oceanic sediments recovered from the hydrate occurrence regions in the ulleung basin, east sea, offshore Korea. Mar Petrol Geol 28(10):1870–1883. https://doi.org/10.1016/j.marpetgeo.2011.02.003

Lee JS, Lee JY, Kim YM, Lee C (2013) Stress-dependent and strength properties of gas hydrate-bearing marine sediments from the ulleung basin, east sea. Korea Mar Petrol Geol 47(11):66–76. https://doi.org/10.1016/j.marpetgeo.2013.04.006.

Li G, Moridis GJ, Zhang K, Li XS (2010) Evaluation of gas production potential from marine gas hydrate deposits in shenhu area of South China Sea. Energ Fuel 24(11):6018–6033. https://doi.org/10.1021/ef100930m

Li G, Moridis GJ, Zhang K, Li XS (2011) The use of huff and puff method in a single horizontal well in gas production from marine gas hydrate deposits in the shenhu area of South China Sea. J Pet Sci Eng 77(1):49–68. https://doi.org/10.1016/j.petrol.2011.02.009

Li G, Li XS, Zhang KN, Li B, Zhang Y (2013) Effects of impermeable boundaries on gas production from hydrate accumulations in the Shenhu area of the South China Sea. Energies 6(8):4078–4096. https://doi.org/10.3390/en6084078

Li CH, Zhao Q, Xu HJ, Feng K, Liu XW (2014) Relation between relative permeability and hydrate saturation in Shenhu area, South China Sea. Appl Geophys 11(2):207–214. https://doi.org/10.1007/s11770-014-0432-6

Li Q, Cheng Y, Zhang H, Yan C, Liu Y (2018) Simulating the effect of hydrate dissociation on wellhead stability during oil and gas development in Deepwater. J Ocean Univ China 17(1):35–45. https://doi.org/10.1007/s11802-018-3544-4

Liu W, Chen Y, Zhu Y, Song Y, Li Y, Li Q (2014) Effects of different mining methods on the strength behavior of gas hydrate-bearing sediments. Energy Procedia 61:547–551. https://doi.org/10.1016/j.egypro.2014.11.1167

Liu J, Zhang JZ, Sun YB, Zhao TH (2017) Gas hydrate reservoir parameter evaluation using logging data in the Shenhu area,South China Sea. Nature Gas GeoScience 28(1):164–172

Masuda YS, Naganawa S, Sato K (1997) Numerical calculation of gas hydrate production performance from reservoirs containing natural gas hydrates. SPE Asia Pacific Oil and Gas Conference, Kuala Lumpur

Masui A, Haneda H, Ogata Y, Aoki K (2005) Effects of methane hydrate formation on shear strength of synthetic methane hydrate sediments. The Fifteenth International Offshore and Polar Engineering Conference, Seoul, pp 364–369

Masui A, Haneda H, Ogata Y, Aoki K (2007) Mechanical properties of sandy sediment containing marine gas hydrates in deepsea offshore Japan survey drilling in Nankai Trough. Seventh ISOPE Ocean Mining Symposium, Lisbon, Portugal, 53–56

Merey S (2016) Drilling of gas hydrate reservoirs. J Nat Gas Sci Eng 35:1167–1179. https://doi.org/10.1016/j.jngse.2016.09.058

Minagawa H, Ohmura R, Kamata Y, Ebinuma T, Narita H, Masuda Y (2005) Water permeability measurements of gas hydrate-bearing sediments. Proc. 5th Int. Conf. Gas Hydrates, Trondheim, Norway

Moridis GJ, Reagan MT (2007) Strategies for gas production from oceanic Class 3 hydrateaccumulations. Offshore Technology Conference, Houston

Ng A, Klar A, Soga K (2008) Coupled soil deformation-flow-thermal analysis of methane production in layered methane hydrate soils. In Proceedings of the Offshore Technology Conference, Houston.

Ning F, Zhang K, Wu N, Zhang L, Li G, Jiang G (2013a) Invasion of drilling mud into gas-hydrate-bearing sediments. Part I: effect of drilling mud properties. Geophys J Int 193(3):1370–1384. https://doi.org/10.1093/gji/ggt015

Ning F, Wu N, Yu Y, Zhang K, Jiang G, Zhang L (2013b) Invasion of drilling mud into gas-hydrate-bearing sediments. Part II: effects of geophysical properties of sediments. Geophys J Int 193(3):1385–1398. https://doi.org/10.1093/gji/ggt016

Qiu K, Yamamoto K, Birchwood RA, Chen YR (2014) Well Integrity Evaluation for Methane Hydrate Production in the Deepwater Nankai Trough. International Petroleum Technology Conference, Kuala Lumpur

Qiu K, Yamamoto K, Birchwood RA, Chen Y (2015) Well-integrity evaluation for methane-hydrate production in the Deepwater nankai trough. SPE Drill Completion 30(1):52–67. https://doi.org/10.2118/174081-PA

Rutqvist J, Moridis GJ (2007) Numerical studies on the geomechanical stability of hydrate-bearing sediments. SPE J 14(2):267–282. https://doi.org/10.2118/126129-pa.

Sakamoto Y, Komai T, Kawamura T, Minagawa H, Tenma N, Yamaguchi T (2007) Laboratory-scale experiment of methane hydrate dissociation by hot-water injection and numerical analysis for permeability estimation in reservoir: part 1-numerical study for estimation of permeability in methane hydrate reservoir. Int J Offshore Polar 17(1):47–56

Schnurle P, Liu C, Hsiuan T, Wang T (2002) Characteristics of gas hydrate and free gas offshore southwestern Taiwan: a combined seismic reflection/refraction analysis. Petroleum Geology of Taiwan 35: 1–33

Shi HH, (2009) The method research of well-bore stability evaluation in shale by logging. Master thesis, China University of Petroleum (East China).

Su Z, Moridis GJ, Zhang K, Yang R, Wu N (2010) SS - Gas Hydrate: Numerical Investigation of Gas Production Strategy for the Hydrate Deposits in the Shenhu Area. Offshore Technology Conference, Houston

Su Z, Cao Y, Wu N, He Y (2011) Numerical analysis on gas production efficiency from hydrate deposits by thermal stimulation: application to the shenhu area, South China Sea. Energies 4(2):294–313. https://doi.org/10.3390/en4020294

Sun S, Ye Y, Liu C, Xiang F, Ma Y (2011) P-t stability conditions of methane hydrate in sediment from South China Sea. J Energy Chem 20(5):531–536. https://doi.org/10.1016/S1003-9953(10)60224-1

Su Z, Huang L, Wu NY, Yang SX (2013) Effect of thermal stimulation on gas production from hydrate deposits in Shenhu area of the South China Sea. Sci China Earth Sci 56(4):601–610. https://doi.org/10.1007/s11430-013-4587-4

Tréhu A, Ruppel C, Holland M, Dickens G, Torres M, Collett T (2006) Gas hydrates in marine sediments: lessons from scientific ocean drilling. Oceanography 19(4):124–142. https://doi.org/10.5670/oceanog.2006.11

Uchida S, Soga K, Yamamoto K (2012) Critical state soil constitutive model for methane hydrate soil. J Geophys Res 117(B3):3209–3221. https://doi.org/10.1029/2011JB008661

Wan Z, Wang X, Xu X, Guo H (2016) Control of marine geothermal field on the occurrence of gas hydrates in northern South China Sea. 2016 SEG International Exposition and Annual Meeting, Dallas, Texas, 1803–1806.

Wang X, Wu S, Lee M, Guo Y, Yang S, Liang J (2011) Gas hydrate saturation from acoustic impedance and resistivity logs in the shenhu area, South China Sea. Mar Petrol Geol 28(9):1625–1633. https://doi.org/10.1016/j.marpetgeo.2011.07.002

Wu NY, Yang SX, Zhang HQ, Liang JQ, Wang HB, Su X, Fu SY (2007) Preliminary discussion on natural gas hydrate reservoir system of shenhu area, north slope of South China Sea. Nat Gas Ind 27(9):1–6

Wu N, Zhang H, Yang S, Zhang G, Liang J, Lu J (2011) Gas hydrate system of shenhu area, northern South China Sea: geochemical results. J Geophys Res 2011:1687–8833. https://doi.org/10.1155/2011/370298.

Xiao K, Zou C, Xiang B, Liu J (2013) Acoustic velocity log numerical simulation and saturation estimation of gas hydrate reservoir in shenhu area, South China Sea. Sci World J 2013:1–13. https://doi.org/10.1155/2013/101459

Yan C, Cheng Y, Li M, Han Z, Zhang H, Li Q (2017) Mechanical experiments and constitutive model of natural gas hydrate reservoirs. Int J Hydrog Energy 42:19810–19818. https://doi.org/10.1016/j.ijhydene.2017.06.135

Yang S, Zhang H, Wu N, Su X, Schultheiss P, Holland M (2008) High concentration hydrate in disseminated forms obtained in shenhu area, north slope of south china sea. In: Proceedings of the 6th International Conference on Gas Hydrates, Vancouver, British Columbia, Canada

Yohan C, Tae S, Young J, Joo Y, Tae-Hyuk K (2016) Geomechanical, hydraulic and thermal characteristics of deep oceanic sandy sediments recovered during the second Ulleung basin gas hydrate expedition. Energies 9(10):775

Zhao ZW (2010) Analysis for multi-field seepage and the deformation of ore body in the process of gas hydrate dissociation. PHD thesis, University of Science and Technology Beijing.

Zhu H, Liu Q, Deng J, Wang G, Xiao X, Jiang Z (2011) Pressure and temperature preservation techniques for gas-hydrate-bearing sediments sampling. Energy 36(7):4542–4551. https://doi.org/10.1016/j.energy.2011.03.053